Regularized Dual-Channel Algorithm for the Retrieval of Soil Moisture and Vegetation Optical Depth from SMAP Measurements

Julian Chaubell, Simon Yueh, Scott Dunbar, Andreas Colliander, Dara Entekhabi, Steven Chan, Fan Chen, Xiaolan Xu, Rajat Bindlish, Peggy O'Neill, Jun Asanuma, Aaron Berg, David Bosch, Todd Caldwell, Michael H. Cosh, Chandra Holifield Collins, Karsten H. Jensen, Jose Martínez-Fernández, Mark Seyfried, Patrick J. Starks, Zhongbo Su, Marc Thibeault and Jeffrey Walker

***Abstract*— In August 2020, SMAP released a new version of its soil moisture (SM) and vegetation optical depth (VOD) retrieval products. In this work, we review the methodology followed by the SMAP regularized dual-channel (DCA) retrieval algorithm. We show that the new implementation generates SM retrievals that not only satisfy the SMAP accuracy requirements but also show a performance comparable to the single-channel algorithm that uses the V polarized brightness temperature (SCA-V). Due to a lack of *in situ* measurements we cannot evaluate the accuracy of the VOD. In this work, we show analyses with the intention of providing an understanding of the VOD product. We compare the VOD results with those from SMOS. We also study the relation of the SMAP VOD with two vegetation parameters: tree height and biomass.**

***Index Terms*— SMAP, soil moisture retrieval, vegetation optical depth retrieval, dual-channel algorithm.**

I. INTRODUCTION

The Soil Moisture Active Passive (SMAP) mission was designed to acquire and combine L-band radar and radiometer measurements for the estimation of soil moisture (SM) with an average unbiased root-mean square error (ubRMSE) of no more than 0.04 m^3/m^3 volumetric accuracy in the top 5 cm of soil for vegetation with water content of less than 5 kg/m^2 [1][2]. SMAP released new versions of its soil moisture (SM) and vegetation optical depth (VOD) products in August 2020. (Version 4 for the L2/3_SM_P_E product and Version 7 for the L2/3_SM_P).

The new implementation of the dual channel algorithm (DCA), which uses the two polarized brightness temperature measurements (H and V), generates SM retrievals, not only satisfying the SMAP accuracy requirements, but also showing a performance comparable to the single-channel algorithm that uses the V polarized brightness temperature (SCA-V) [2][3][4].

While the accuracy of the DCA SM can be evaluated by comparison with *in situ* data, the lack of VOD *in situ* data raises concerns about the accuracy of the VOD product. Although the SMAP mission does not have a requirement for the accuracy of the retrieved VOD, it is of great value for the SMAP team and the science community in general since it provides critical information about the water content of the aboveground biomass and its seasonal variations. In order to understand the performance of the VOD product, it is common to compare it to similar products from other missions and to look at it in

The manuscript was submitted on May 30, 2021. The work described in this paper was carried out by the Jet Propulsion Laboratory, California Institute of Technology under a contract with the National Aeronautics and Space Administration.

Julian Chaubell, Steven Chan, Scott Dunbar, Andreas Colliander Simon Yueh and Xiaolan Xu, are with the Jet Propulsion Laboratory, California Institute of Technology, Pasadena, CA 91109 USA. (email: julian@jpl.nasa.gov; Steventsz.K.Chan@jpl.nasa.gov; Roy.S.Dunbar@jpl.nasa.gov; Andreas.Colliander@jpl.nasa.gov; simon.yueh@jpl.nasa.gov; Xiaolan.Xu@jpl.nasa.gov)

Fan Chen is with SSAL Inc., Greenbelt, MD and USDA Agricultural Research Service, Beltsville, MD, USA (email: fan.chen@ars.usda.gov)

Dara Entekhabi is with the Massachusetts Institute of Technology, Cambridge, Massachusetts, USA (email: darae@mit.edu).

Rajat Bindlish and Peggy O'Neill are with the Goddard Space Flight Center, Greenbelt, MD, USA. (email: rajat.bindlish@nasa.gov; peggy.e.oneill@nasa.gov).

Jun Asanuma is with Center for Research in Isotopes and Environmental Dynamics (CRiED), Tsukuba University (email: asanuma@ied.tsukuba.ac.jp).

Aaron Berg is at the Department of Geography, Environment and Geomatcis at the University of Guelph (email: aberg@uoguelph.ca).

David D. Bosch is with USDA Agricultural Research Service Southeast Watershed Research (email: David.Bosch@usda.gov).

Todd Caldwell is with U.S. Geological Survey, Nevada Water Sciences Center (email: tcaldwell@usgs.gov).

Michael H. Cosh is with USDA Agricultural Research Service, Beltsville Agricultural Research Center, Hydrology and Remote Sensing Laboratory (email: michael.cosh@usda.gov)

Chandra Holifield Collins is with USDA Agricultural Research Service Southwest Watershed Research (email: Chandra.Holifield@ars.usda.gov).

Karsten H. Jensen is with the University of Copenhagen, Copenhagen, Denmark. (email: khj@ign.ku.dk).

Jose Martínez-Fernández is with Instituto Hispano Luso de Investigaciones Agrarias (CIALE), Universidad de Salamanca (email: jmf@usal.es).

Mark Seyfried is with USDA Agricultural Research Service Northwest Watershed Research Center (email: Mark.Seyfried@ars.usda.gov).

Patrick J. Starks is with USDA Agricultural Research Service Great Plains Agroclimate and Natural Resources Research Unit (email: patrick.starks@usda.gov).

Zhongbo Su is with ITC Faculty, University of Twente (email: z.su@utwente.nl).

Marc Thibeault is with Comisión Nacional de Actividades Espaciales (CONAE) (email: mthibeault@conae.gov.ar).

Jeffrey Walker is with Monash University, Australia (email: jeff.walker@monash.edu.au).

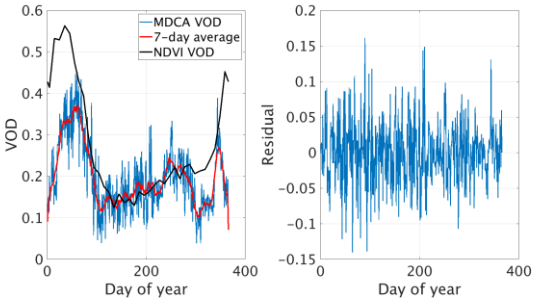

(a) (b)

Fig. 1 Climatology over Monte Buey (lat -32.91, lon -62.51) SMAP CVS (a). Residual obtained by subtracting the 7-day average and the MDCA climatology (b). The residual with seasonal variation removed is used to compute λ = 1/ σ. The NDVI climatology shown on the (a) (black curve) shows the selected initial guess over that CVS

relation to other vegetation parameters such as tree height and biomass.

Recent efforts to retrieve SM and VOD from SMAP L-band brightness temperature data have resulted in significant progress [5]. Reference [5] uses a multi-temporal dual channel algorithm (MT-DCA), which assumes that VOD changes more slowly than SM and can be assumed to be almost constant between every two consecutive overpasses. In addition, the MT-DCA approach allows for the retrieval of a single temporally constant value of the scattering albedo per pixel. The Soil Moisture and Ocean Salinity (SMOS) mission [6], produces simultaneous retrievals of SM and VOD based on angular information in its V- and H-pol brightness temperature products. Its L-band VOD retrievals have been analyzed by several authors [7][8][9]. SMOS-IC [10] presented an

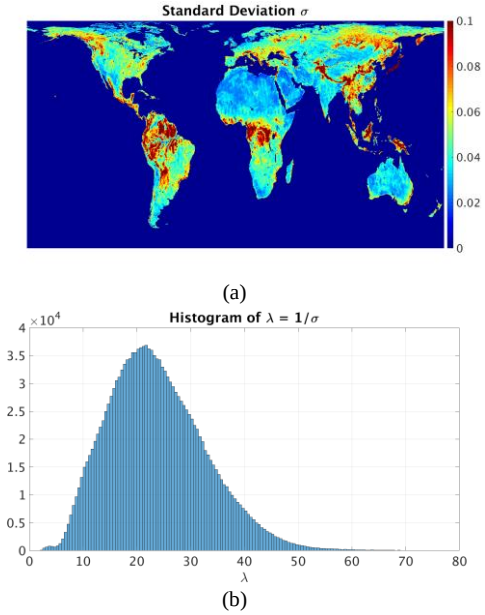

(a)

(b)

Fig. 2 Global map of σ (top) from the residuals as in Fig. 1. At the bottom the histogram of the corresponding λ. The histogram shows the peak value at λ=20.

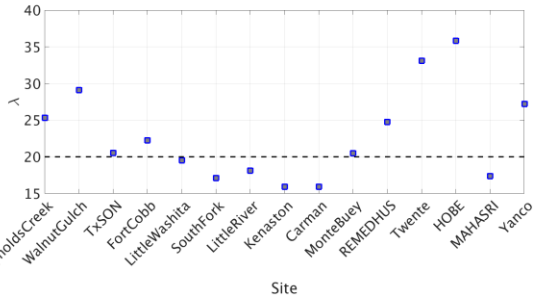

Fig. 3 Values of λ at each CVS used to evaluate RDCA- λ

alternative approach to the retrieval of the SM and VOD but is still using angular brightness temperature information.

In this presented work, we detail the methodology for the DCA implementation in section II. In section III we present results of retrieved SM over Core Validation Sites (CVS) [4], [19], [20], [21], [22], [23], [24], [25], [26], [27], [28], [29], [30], and the sparse network (SP) [17], [18]. We also present VOD results in section III. In section IV we compare the SMAP VOD with the vegetation parameters, including tree height and biomass. In section V we compare the SMAP VOD results with those obtained by SMOS.

II. REGULARIZED DUAL-CHANNEL ALGORITHM

The newly implemented DCA simultaneously retrieves the SM and VOD (τ_θ) by minimizing the cost function

$$F_D(SM,\tau_\theta) = \left[TB_V^{sim}(SM,\tau_\theta) - TB_V^{obs}\right]^2 + \left[TB_H^{sim}(SM,\tau_\theta) - TB_H^{obs}\right]^2 + \lambda^2(\tau_\theta - \tau^*)^2, \quad (1)$$

where TB_V^{sim} is the V-polarized simulated brightness temperature and TB_H^{sim} is the H-polarized simulated brightness temperature, λ is a regularization parameter and τ^* an initial expected VOD value.

To simulate the L-band emission of the soil-vegetation system the SMAP team uses the zero-order approximation of the radiative transfer equations, known as the τ-ω emission model [10]. The brightness temperature equation, which includes emission components from the soil and the overlying vegetation canopy, is given by

$$TB_p^{sim} = T_s e_p exp(-\tau_p sec\,\theta) + T_c(1-\omega_p)[1 - exp(-\tau_p sec\,\theta)][1 + r_p exp(-\tau_p sec\,\theta)] \quad (2)$$

where the subscript p refers to polarization (V or H), T_s is the soil effective temperature, T_c is the vegetation temperature, τ_p is the nadir vegetation opacity, ω_p is the vegetation effective scattering albedo, r_p is the rough soil reflectivity, e_p is the rough soil emissivity and θ is the incidence angle.

The surface roughness reflectivity is modeled by

$$r_p(\theta) = [(1-Q)r_p^*(\theta) + Q r_q^*(\theta)]e^{(-h\,cos^N(\theta))} \quad (3)$$

TABLE I
ACRONYMS SUMMARY

Algorithm	Description
DCA	Dual-channel algorithm. It uses the two polarized brightness temperature measurements (H and V) to simultaneously retrieve SM and VOD. General algorithm name.
MDCA	Modified dual-channel algorithm [3]. This implementation includes changes in the roughness reflectivity model with respect to the original SMAP DCA implementation. No regularization is applied.
RDCA	Modified dual-channel algorithm with regularization. Regularization parameter λ = 20 globally. In August 2020 we renamed the modified dual-channel algorithm to DCA which corresponds to the RDCA configuration.
RDCA-λ	Modified dual-channel algorithm with regularization. Regularization parameter varying globally.

where Q (polarization decoupling factor which is related to h by the linear relation $Q = 0.1771\ h$), h, and N are the roughness parameters and $r_p^*(\theta)$ is the Fresnel reflectivity of the smooth surface where the index p and q (q opposite to p) account for the polarization V or H. The baseline SMAP implementation of the retrieval algorithms assumes that in Eq. (2) $T_s = T_c$ at the early morning descending overpass and that $\omega_p = \omega$ and $\tau_p = \tau$ are polarization independent to reduce the number of algorithm parameters [2]. Note that in Eq. (1) τ_θ is related to the nadir vegetation opacity by $\tau_\theta = \tau\ sec\ \theta$.

The implementation of Eq. (1), Eq. (2) and Eq. (3) requires that several parameters need to be assumed: *a prior* value of the scattering albedo based on land cover, roughness parameters as detailed in [3], effective soil temperature, clay fraction to determine the soil dielectric constant, as well as the regularization parameters τ^* and λ [2].

A. *Selection of parameter λ*

The retrieval of VOD through the DCA algorithm with λ=0 (MDCA, modified DCA [3]) produces VOD results with high variability in the temporal dimension as shown in Fig. 1 (a) (blue curve) and also in the spatial dimension. Fig. 1 (a) displays an example of the MDCA climatology at the Monte Buey CVS. It also shows the 7-day average and the VOD based on Normalized Difference Vegetation Index (NDVI) climatology from the Moderate-Resolution Imaging Spectroradiometer (MODIS). The selection of λ determines how much the residual noise (Fig 1 (b)) will be suppressed and how much freedom the optimization algorithm will have to converge to a solution of VOD apart from the expected value τ^*. Indeed, the value of λ=0 means no regularization and very high values of λ will force the retrieval of VOD to converge to τ^*.

To select potential candidates of λ we considered 5 years (04/01/2015 - 03/31/2020) of MDCA VOD data for each 9km EASE-2 (Equal Area Scalable Earth Grid version 2) grid cell and computed its daily climatology, Fig. 1 (a). To remove the seasonal variation, we computed a 7-day average (red curve in Fig. 1 (a)) which is subtracted from the MDCA climatology resulting in the residual shown in Fig 1 (b). We used the standard deviation (σ) of the residual to determine the amount of regularization needed and defined λ as 1/ σ. Fig. 2 displays a global map of σ (top) and the histogram of the corresponding λ (bottom). Fig.2 shows that σ varies across the globe and that the histogram peaks at λ~=20.

We evaluated the performance of the SM retrievals compared to *in situ* SM data from 15 SMAP CVS by setting λ=20 fixed over all the sites and also using the local values of lambda over each CVS. Fig. 3 displays the values of lambda for each CVS. In what follows we will refer to RDCA for the regularized DCA algorithm with regularization parameter λ=20 and RDCA-λ for the regularized DCA algorithm with λ changing spatially.

Table I summarize the acronyms used to differentiate the different DCA implementations.

Table II shows the algorithm performance metrics for SM retrievals. The metrics are the average of those at each CVS. The metrics show that even though a non-zero lambda is crucial to get good performance by the DCA algorithm, the selection of the values of λ is not relevant as long as λ is allowed to vary locally about the value λ=20. For this reason and considering the ease of the operational implementation we decided to set λ=20 globally.

TABLE II
RDCA, RDCA-λ PERFORMANCE COMPARISON

Alg.	ubRMSE	RMSE	Bias	Corr.	MaBias
RDCA	0.36	0.46	-0.010	0.819	0.037
RDCA-λ	0.36	0.47	-0.009	0.821	0.038

Performance analysis of soil moisture retrievals over SMAP CVS for λ=20 (RDCA) or the corresponding local values (RDCA-λ). as in Fig. 2.

B. *Selection of the initial guess τ^**

As an initial guess τ^* , an estimate of VOD based on NDVI climatology was selected [2]. This selection aroused concerns regarding how the seasonal behavior of the RDCA VOD would be affected.

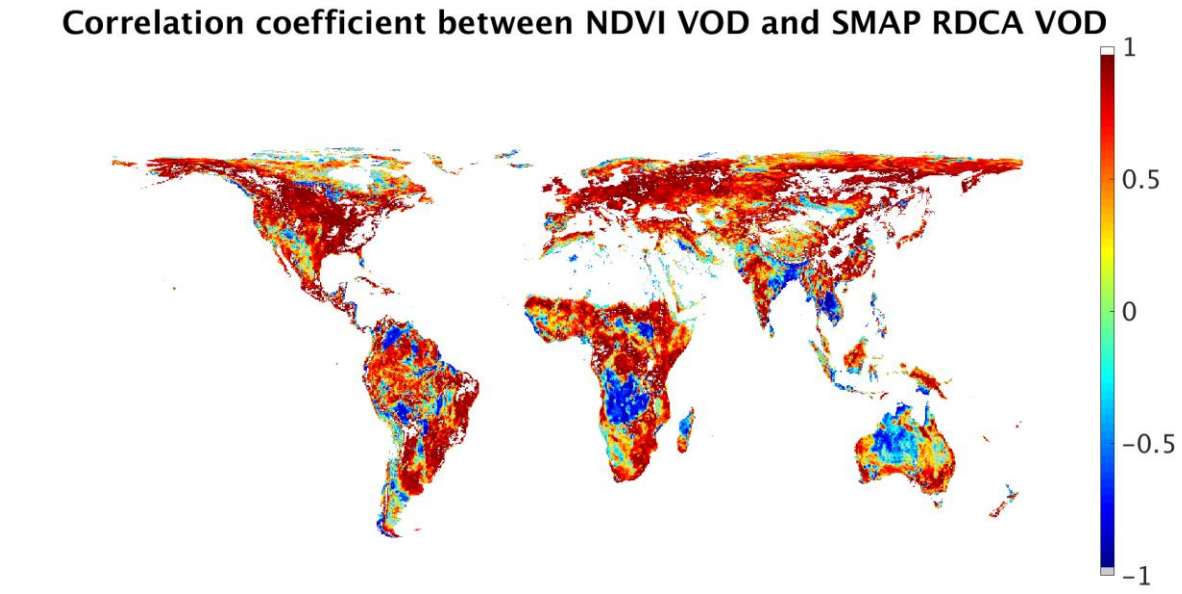

(a)

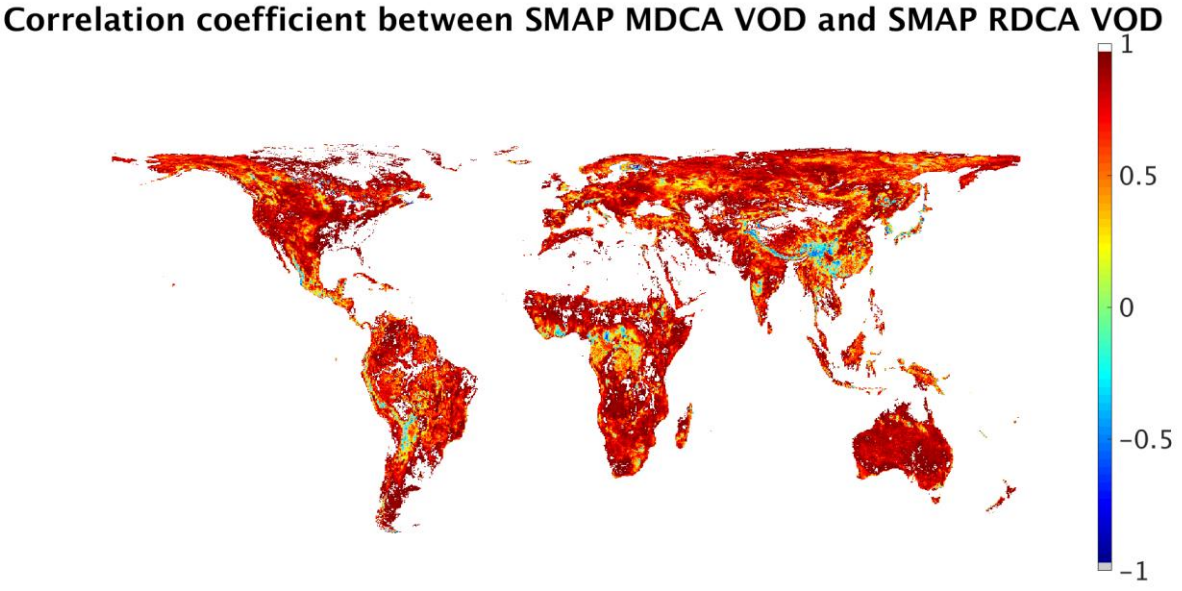

(b)

Fig. 4 Correlation map between NDVI VOD and RDCA VOD (a) and between RDCA VOD and MDCA VOD (b). Grey areas indicate pixel with p-values>0.05. White areas indicate not available data

To address this, we compared the Pearson correlation of the daily climatology of RDCA VOD with daily climatology of NDVI VOD (Fig. 4 (a)) and daily climatology of MDCA VOD (Fig. 4 (b)). The figure shows that while the correlation between RDCA VOD and the NDVI VOD is moderate (mean value of 0.51 and standard deviation of 0.51), there is a high correlation globally between RDCA VOD and MDCA VOD (mean value of 0.76 and standard deviation of 0.25) which is an indication that RDCA VOD follows the MDCA VOD seasonal variation more consistently than the seasonal variation of the NDVI VOD. We also looked into the time difference (in days) between the NDVI τ^* peak location (in Fig. 1, black curve) and the peak location of the RDCA VOD climatology (in Fig. 1, red curve) and similarly for MDCA VOD and RDCA VOD. Fig. 5 displays the histograms of differences. We can see that while the differences are widespread for NDVI τ^*minus RDCA VOD, for RDCA VOD – minus MDCA VOD most of the values concentrate around zero. This is another indication that both MDCA VOD and RDCA VOD reach their maximum value at approximately the same time. These two tests suggest that in general the use of the NDVI τ^* does not affect the seasonal variation of the MDCA VOD significantly.

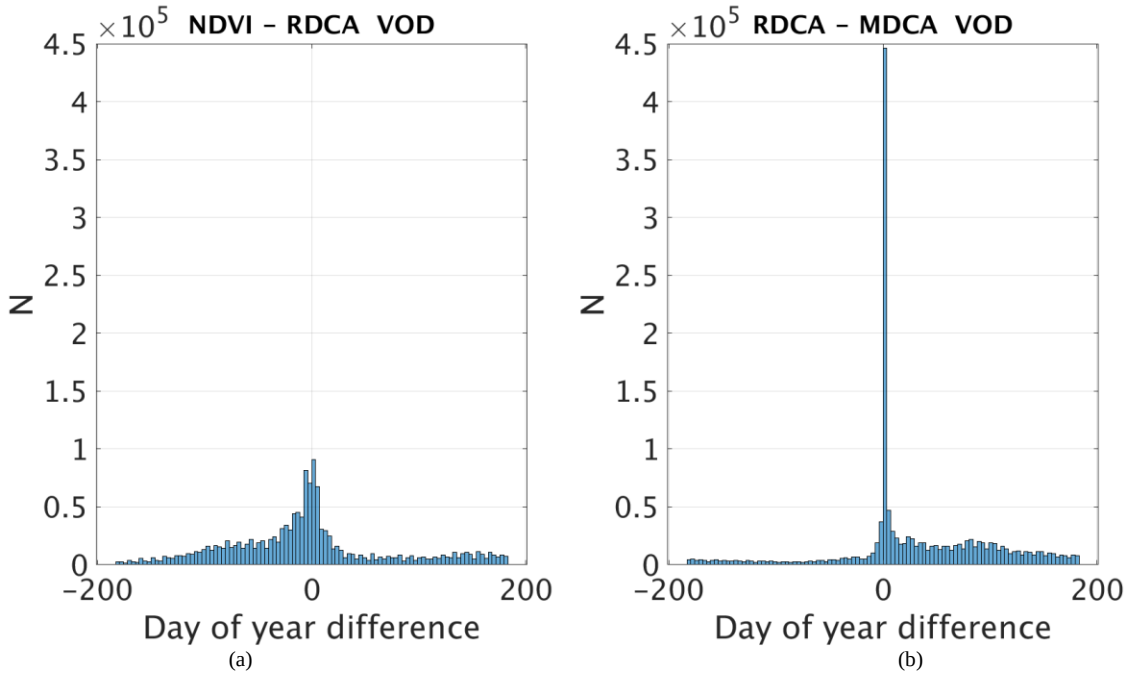

Fig. 5 Time differences of vegetation peak occurrence in days. (a) Difference between NDVI VOD and SMAP RDCA VOD. (b) Difference between SMAP RDCA VOD and MDCA VOD

III. ASSESSMENT

The SMAP mission validates the accuracy of the retrieved SM using several sources of information [15]. Among them are CVS which provide the ground-based data in a timely manner to the SMAP project, and sparse networks such as the USDA Soil Climate Analysis Network (SCAN) [16], the NOAA Climate Research Network [17] and the Oklahoma Mesonet [18].

Table III shows how the SCA-V, MDCA and RDCA soil moisture retrievals compare at the CVS. We can see that a significant improvement has been reached by the implementation of the regularization term in the DCA algorithm. The table also shows that the RDCA and SCA-V are statistically similar.

Table IV displays the assessment report over the sparse networks using 5 years of SMAP SM data (2015/01/04-2020/03/31). The table compares the accuracy of MDCA, SCA-V and RDCA. We display ubRMSE, bias, and correlation (R) for several land cover types: Evergreen needleleaf forest, Open shrublands, Woody savannas, Savannas, Grasslands, Croplands, Crop/Natural vegetation mosaic and Barren/Sparse. We observe again that SCA-V and RDCA present similar performance and that RDCA shows a significant improvement

TABLE III
ASSESSMENT OF SOIL MOISTURE RETRIEVALS OVER CVS

Descending												
Algorithm	MDCA				SCA-V				RDCA			
	ubRMSE	Bias	RMSE	R	ubRMSE	Bias	RMSE	R	ubRMSE	Bias	RMSE	R
Mean	0.041	-0.006	0.052	0.762	0.038	-0.006	0.048	0.814	0.036	-0.009	0.045	0.815
Ascending												
Algorithm	MDCA				SCA-V				RDCA			
	ubRMSE	Bias	RMSE	R	ubRMSE	Bias	RMSE	R	ubRMSE	Bias	RMSE	R
Mean	0.041	-0.006	0.052	0.762	0.037	-0.008	0.048	0.807	0.036	-0.013	0.045	0.787

CVS assessment of soil moisture retrievals. 5 years (04/01/2015-03/31/2020) of data were used to compare the accuracy of MDCA with SCA-V and RDCA. We display the averaged RMSE(m^3/m^3), ubRMSE(m^3/m^3), Bias(m^3/m^3) and correlation (R) over 15 SMAP CVS.

TABLE IV
ASSESSMENT OF SOIL MOISTURE RETRIEVALS OVER SPARSE NETWORK

Descending												
Algorithm	MDCA				SCA-V				RDCA			
	ubRMSE	Bias	RMSE	R	ubRMSE	Bias	RMSE	R	ubRMSE	Bias	RMSE	R
Mean	0.049	0.008	0.070	0.660	0.048	-0.001	0.069	0.659	0.047	0.006	0.070	0.667
Ascending												
Algorithm	MDCA				SCA-V				RDCA			
	ubRMSE	Bias	RMSE	R	ubRMSE	Bias	RMSE	R	ubRMSE	Bias	RMSE	R
Mean	0.049	0.009	0.071	0.623	0.047	0.002	0.069	0.633	0.047	0.007	0.069	0.639

Sparse Network assessment of soil moisture retrieval. 5 years (04/01/2015-03/31/2020) of data were used to compare the accuracy of MDCA (DCA with $\lambda=0$) with SCA-V (single channel algorithm with V polarization measurement of brightness temperature) and RDCA (DCA with $\lambda=20$). We display the averaged RMSE(m^3/m^3), ubRMSE(m^3/m^3), Bias(m^3/m^3) and correlation (R) over several land cover types.

with respect to MDCA. A thorough analysis of the SMAP soil moisture performance can be found in [4]

IV. SMAP VOD VS TREE HEIGHT AND BIOMASS

In this section we analyze the correlation between the SMAP RDCA VOD and two vegetation parameters: tree height in unit of meters (m) [13] and the aboveground biomass density of vegetation in units of Mg/ha [14]. Both sets of data were aggregated to the 9km EASE-2 to match the enhanced SMAP data, Fig. 6.

Fig. 7 (a) displays the density plots of VOD vs tree height and Fig. 7 (b) and (c) displays VOD vs biomass. Fig. 7 also

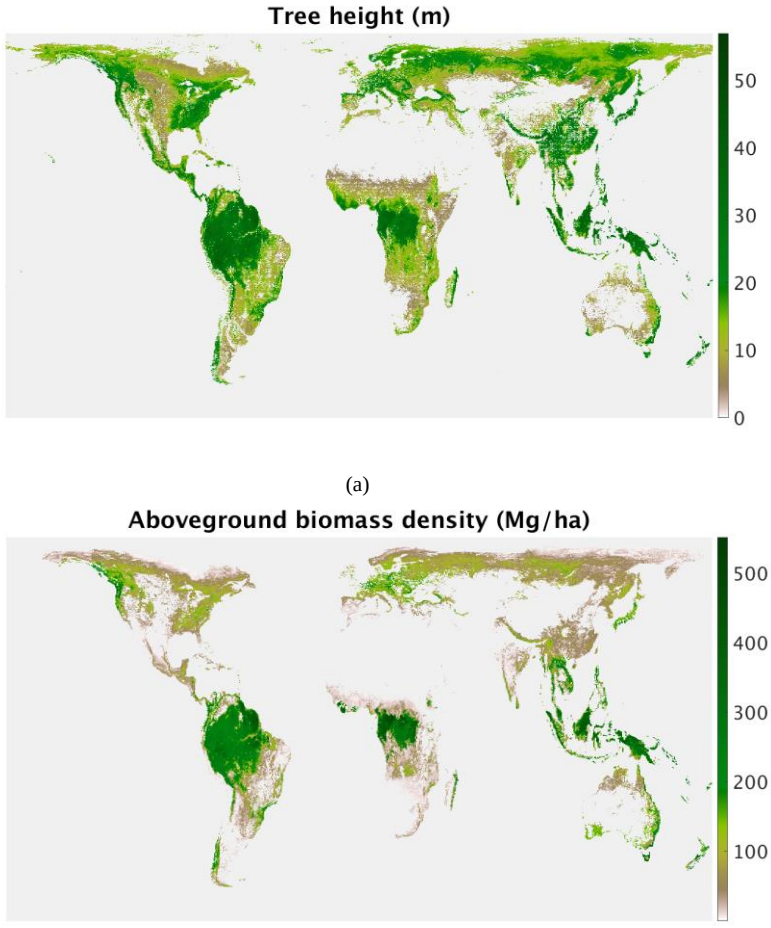

(a)

(b)

Fig. 6. (a) Tree height (meters). (b) aboveground biomass density of vegetation in units of Mg/ha

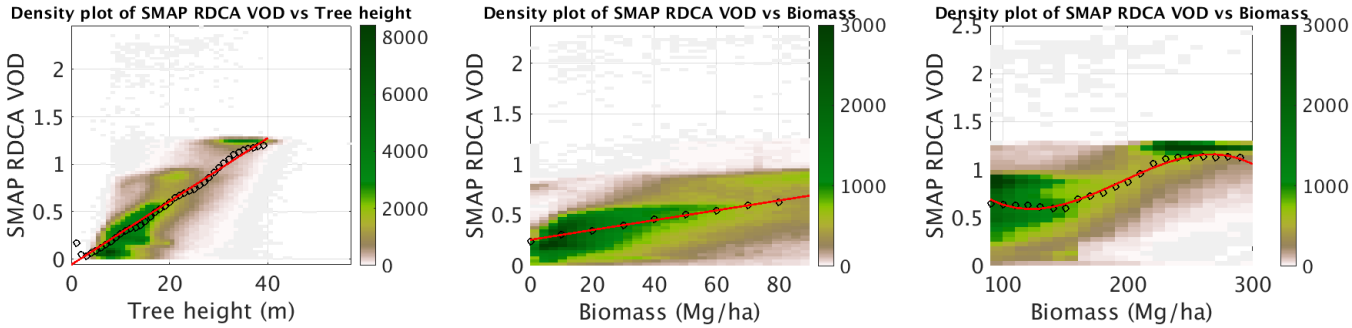

(a) (b) (c)

Fig. 7. Density plots and mean fitting curves. (a) SMAP RDCA VOD vs Tree height. (b) SMAP RDCA VOD vs Biomass for values of biomass less than 90 Mg/ha. (c) SMAP RDCA VOD vs Biomass for values of biomass greater than 90 Mg/ha and less than 300 Mg/ha.

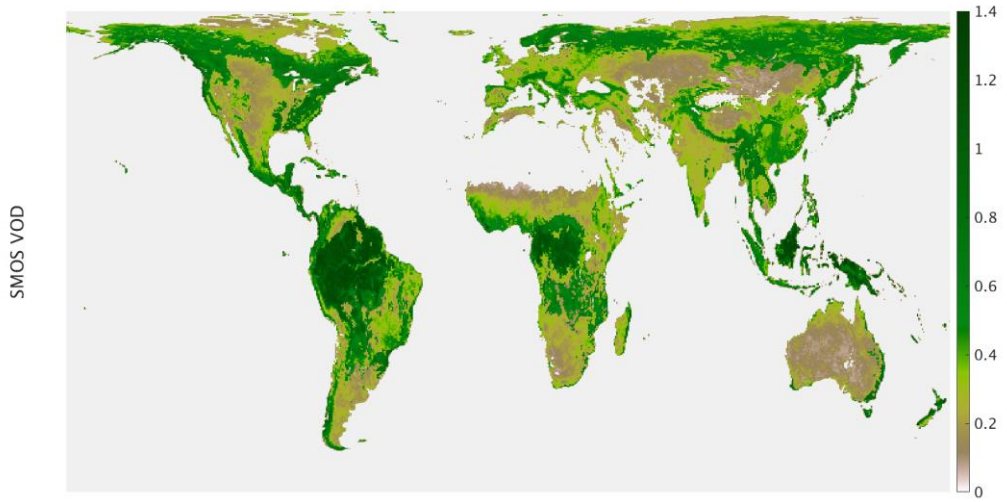

(a)

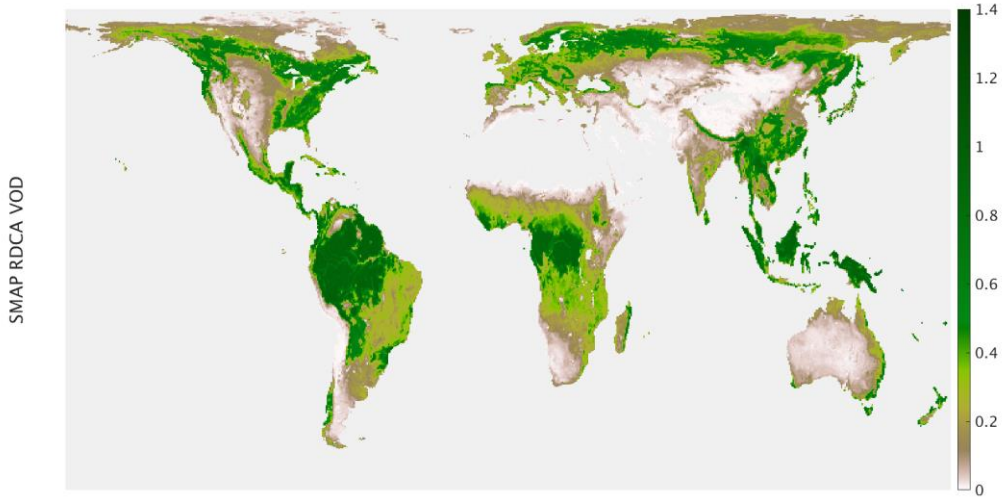

(b)

Fig. 8. Global maps of averaged SMOS VOD (a) and SMAP RDCA VOD (b) for 5 years of data (04/01/2015-03/31/2020).

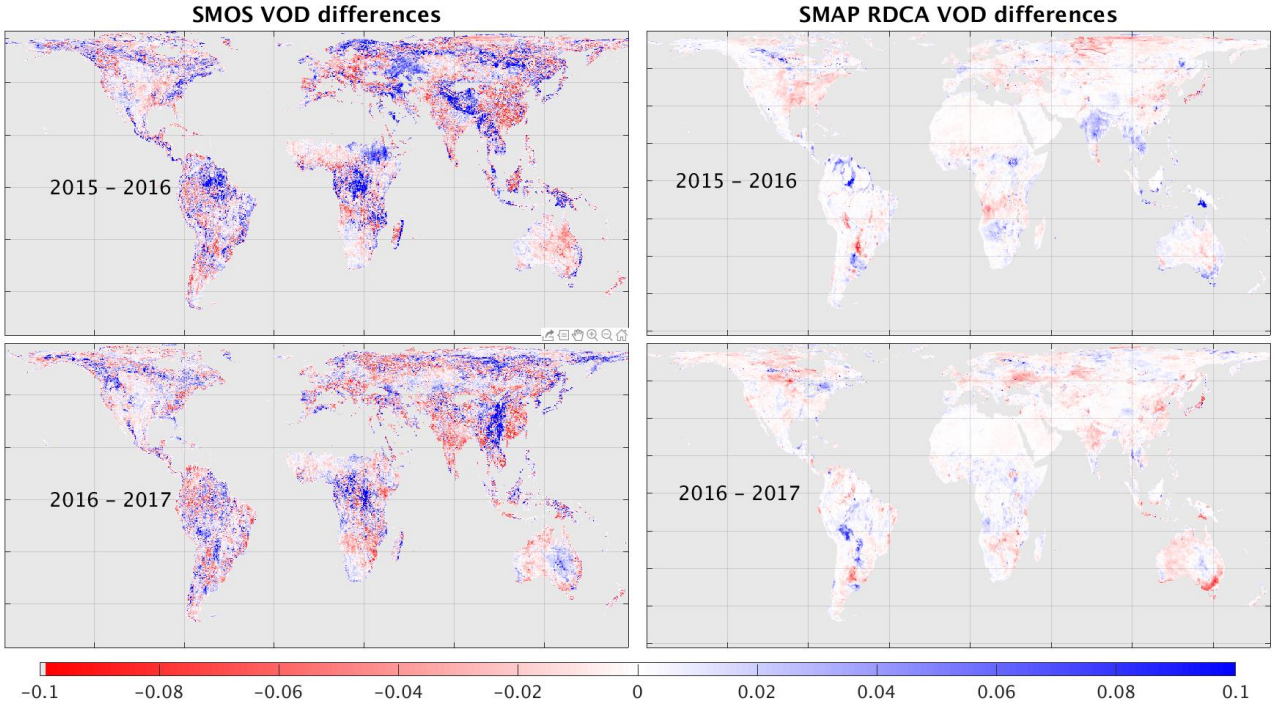

Fig. 9. VOD difference for two consecutive years. 2015-2016 on top and 2016-2017 on the bottom.

displays the mean values for several bins and the fitting curve. To compute the mean values, the data were binned by intervals of tree height of 1 m and the biomass by intervals of 10 Mg/ha.

There is clear linearity between SMAP RDCA VOD and tree height spatially for values of tree height less than 20 m and the relationship remains fairly linear up to tree heights of ~ 35 m/ The slope of the fitting curve is 0.033 and the offset is -0.06. The spatial correlation between SMAP RDCA VOD and the tree height map is R = 0.81 (strong).

The VOD vs biomass density plot (Fig.7 (b)) also shows linearity for values of biomass less than 90 Mg/ha. The VOD vs biomass (B) fitting curve for values of *B* between 0 and 90 Mg/ha is given by:

$$vod = 0.004854\, B + 0.2541 \qquad (4)$$

For values of biomass greater than 90 Mg/ha and less than 150 Mg/ha the VOD stays almost constant, this could be caused by a reduction in the amount of data points together with an increase in dispersion. Fig 7. (c) shows that after *B* values of 150 Mg/ha the VOD starts increasing again and reaches saturation at about *B* values of 240 Mg/ha.

Heterogeneity of the grid pixel could be one of the factors causing the scatter in the density plots. The spatial correlation between the SMAP VOD and the biomass map is R = 0.53 (moderate).

V. SMAP RDCA VOD vs SMOS VOD

The lack of VOD *in situ* data makes it difficult to evaluate the accuracy and performance of the SMAP RDCA VOD product. In order to understand the performance of the VOD product we compare the SMAP RDCA VOD product (L2_SM_P_E v4 [12]) with the SMOS Level 3 VOD (ftp://ftp.ifremer.fr/Land_products/GRIDDED/L3SM/). For comparison, the SMAP RDCA VOD product was multiplied by $\cos(40^o)$ to match the SMOS VOD product at nadir.

Fig. 8 displays global maps of VOD. The SMAP data were aggregated to the 25km EASE-2 grid to match the SMOS data. We observed that the SMOS VOD has higher values of VOD. In fact, the mean VOD and standard deviation for the SMOS are 0.42 and 0.28 respectively, while for SMAP, those values are 0.29 and 0.26 respectively. This difference in value may be caused by different levels of the roughness parameters used by the two missions. Table V presents the mean and standard deviation for SMOS, SMAP and the NDVI VOD by land cover type following the MODIS-based IGBP (International Geosphere Biosphere) classification. For the computation of the statistics, we considered only pixels with Gini-Simpson-Index (GSI) less than 0.1. The GSI is commonly used in ecology as a measure of degree of homogeneity, where GSI = 0 means total homogeneity and is computed as:

$$GSI = 1 - \sum_{i=1}^{n} f_i^2 \qquad (5)$$

where f_i is the fraction of the area covered by the i-th land use classification and *n* is the number of land cover types. Table V shows that in general there is very good agreement between the magnitude of the SMAP RDCA VOD and the magnitude of the NDVI VOD. This is somehow expected due to the nature of the roughness parameter *h* implemented by the SMAP algorithm [3]. In the τ-ω emission model τ and *h* cannot be seen as parameter independent of each other and the magnitude of the

TABLE V
SMAP AND SMOS STATISTICS COMPARISON BY LAND COVER TYPE

Land cover type	SMOS mean	SMAP mean	NDVI mean	SMOS std	SMAP std	NDVI std	N
Evergreen needleleaf forest	0.64	0.62	0.64	0.12	0.08	0.07	598
Evergreen broadleaf forest	1.08	0.91	0.93	0.20	0.07	0.05	12295
Deciduous needleleaf forest	0.54	0.44	0.45	0.10	0.02	0.02	762
Deciduous broadleaf forest	0.71	0.64	0.65	0.13	0.06	0.06	363
Mixed forest	0.64	0.66	0.67	0.12	0.08	0.04	2204
Closed shrublands	NaN	NaN	NaN	NaN	NaN	NaN	0
Open shrublands	0.24	0.07	0.07	0.14	0.06	0.05	16734
Woody savannas	0.54	0.37	0.42	0.18	0.05	0.04	3403
Savannas	0.31	0.24	0.26	0.12	0.05	0.05	4005
Grasslands	0.19	0.04	0.06	0.09	0.03	0.04	10900
Permanent wetlands	0.39	0.07	0.07	0.38	0.16	0.17	10
Croplands	0.25	0.12	0.18	0.06	0.05	0.04	4923
Urban and built-up	0.28	0.10	0.23	0.05	0.14	0.02	4
Crop/Natural vegetation mosaic	0.33	0.25	0.29	0.17	0.12	0.11	243
Snow and ice	0.33	0.04	0.03	0.27	0.04	0.05	17705
Barren/Sparse	0.18	0.01	0.00	0.11	0.00	0.00	23565

Statistics of SMAP, SMOS and NDVI VOD by land cover type classification. N represents the number of pixels involved in the computation. Pixels with GSI < 0.1 were considered.

selected *h* will affect the magnitude of the retrieved τ. Since the values of *h* are obtained by a DCA type algorithm involving NDVI τ as an input, we expect to have retrieved values of τ of magnitude similar to the NDVI τ. However, since the values of *h* are temporal invariant, the seasonality variation of τ should not be affected.

Table V also shows that there is very good agreement with SMOS VOD over forested areas although SMOS data seem to have more variability. In fact, SMOS data seem to have more variability for all the land cover types except for Urban and built-up settings. For land cover types other than forest we observed significant discrepancies in the statistics between SMOS and SMAP RDCA VOD.

Fig. 9 displays the VOD differences for two consecutive years: 2015-2016 and 2016-2017. SMAP RDCA VOD tracks yearly changes in VOD unlike the NDVI VOD which is a ten-year climatology. The SMOS VOD product exhibits more variability than the SMAP RDCA VOD. SMAP RDCA VOD is smoother due to the use of NDVI VOD as regularization

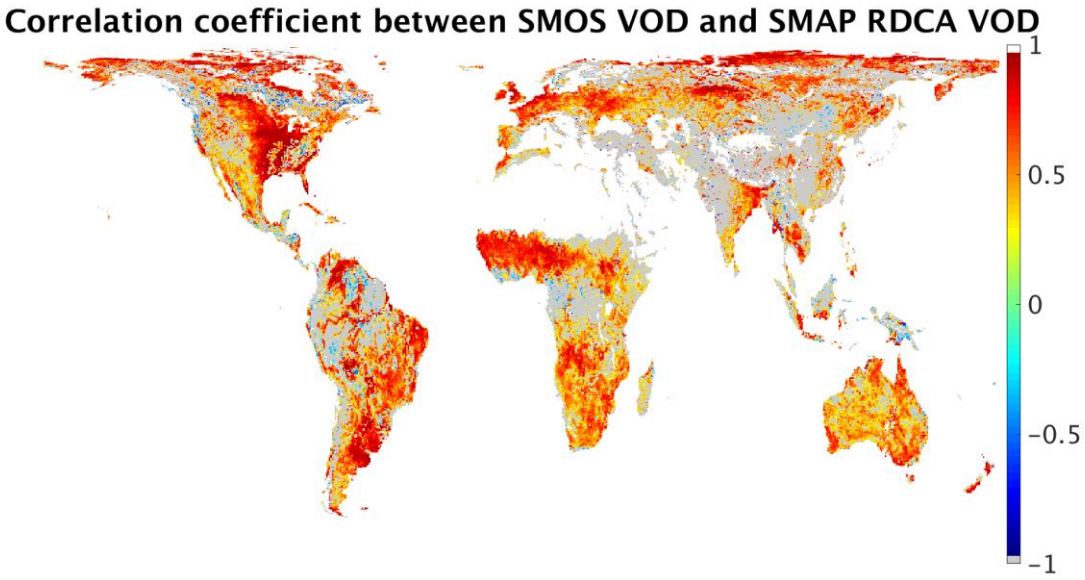

Fig. 10. Map of Pearson correlation between monthly averaged SMOS and SMAP RDCA VOD. Grey areas indicate pixel with p-values>0.05. White areas indicate not available data

TABLE VI
SMAP VS SMOS VOD CORRELATION BY LAND COVER

ENF	EBF	DNF	DBF	MF	CS	OS	WS	S	G	PW	C	UB	CNVM	SI	BS
0.306	0.363	0.531	0.472	0.503	0.300	0.543	0.511	0.576	0.566	0.723	0.631	0.582	0.620	0.605	0.340

SMAP RDCA VOD vs SMOS VOD monthly timeseries Pearson correlation by land cover types as defined by the IGBP land cover classification (land cover abbreviations from Table 4). The analysis was performed only for pixels with significant correlation p-value<0.05

parameter τ^*. There are some similarities between SMOS and SMAP but also some
discrepancies. For example, over Australia, in Fig. 9 (top row), the trends seem to agree although SMOS shows greater differences. On the other hand, in Fig. 9 (bottom row) over the same region the trends are distinctly different except for a portion in the east-central part of the country. We also see discrepancies in Fig. 9 (top row) for the east coast of the United States.

Fig. 10 displays the Pearson correlation (R) between SMAP and SMOS VOD. The aggregated SMAP RDCA VOD and the SMOS VOD were averaged monthly, thus obtaining two data sets of dimensions (1388,584,60) and then for each grid cell the temporal correlation was obtained. We observed that the correlation varies along the globe with a mean value of 0.344 (weak correlation) and standard deviation of 0.33. If we only consider correlation with p-values < 0.05 then the mean correlation value is 0.542 (moderate correlation) and the standard deviation is 0.26. It is noticeable that the correlation is mostly positive indicating a degree of agreement in trends. Table VI displays the correlation by land cover types using only pixels with significant correlation, p-value < 0.05. We observed mostly moderate correlation, with the exception of Permanent wetlands (PW) where the correlation is strong and Evergreen needleleaf forest (ENF), Evergreen broadleaf forest (EBF), Closed shrublands (CS) and Barren/Sparse (BS) where the correlation is weak. Fig. 11 displays the monthly average of VOD at five different regions. From top to bottom the regions are:

1) Peruvian Amazonia [-4.5 -4 -75 -74.5], land cover type: Evergreen broadleaf forest. The SMOS-SMAP correlation is very week R = 0.148 and p-value > 0.05.
2) Angola [-12.5 -12 17 17.5], land cover type: Woody savannas. The SMOS-SMAP correlation is strong R = 0.806 and p-value < 0.05.
3) South Fork, Iowa [42 42.5 -93.5 -93], land cover type: Croplands. The SMOS-SMAP correlation is strong R = 0.873 and p-value < 0.05.
4) Zambia [-14.5 -14 24 24.5], land cover type: Woody savannas. The SMOS-SMAP correlation is moderate R = 0.435 and p-value < 0.05.
5) Chaco, Argentina [-25.5 -25 -62.5 -62], land cover type: Deciduous broadleaf forest. The SMOS-SMAP correlation is strong R = 0.747 and p-value < 0.05.

We see that in all the cases the SMOS and SMAP have consistent trends while NDVI VOD trends only agree with SMAP and SMOS over Chaco and South Fork. There is a big difference in the VOD magnitude over the Peruvian Amazonia

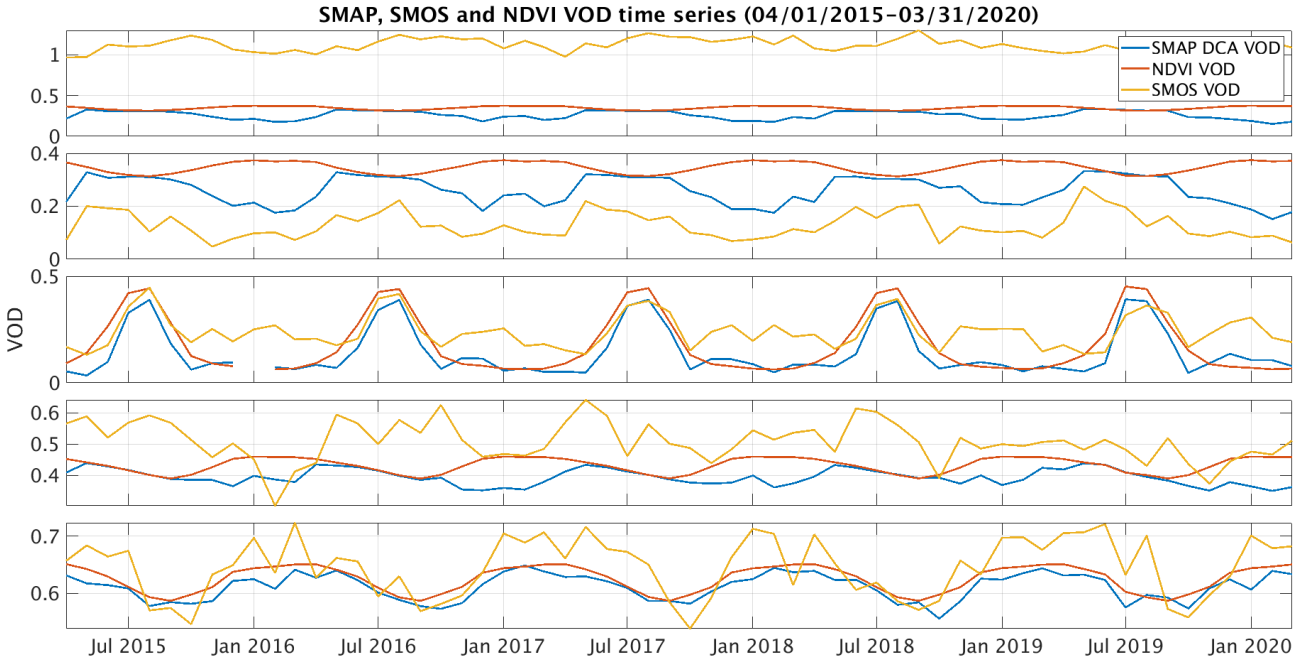

Fig. 11. Sixty months (04/2015-03/2020) of averaged VOD (SMAP, SMOS and NDVI) for 5 different regions. From top to bottom: Peruvian Amazonia, Angola, South Fork (Iowa), Zambia and Chaco (Argentina).

and very weak correlation caused by the low seasonal change of VOD combined with the differences in short term variability. The correlation is not significant according to the p-value (we consider a correlation to be significant if the p-value is < 0.05). We also observed that the SMOS VOD has more variability which may be the cause of low correlation in some locations, as can be seen in the Zambia case, Fig. 11 second from the bottom.

The spatial correlation between SMOS VOD and SMAP RDCA VOD as shown in Fig. 8 is R = 0.83 (strong).

VI. CONCLUSION

In this work, we have shown that the regularized DCA algorithm (RDCA along this paper) implemented in the new release (R17) allows for an accurate retrieval of SM and a reliable VOD (τ). Indeed, we showed that the DCA SM not only satisfies the SMAP requirements but also showed accuracy levels comparable to the SMAP SCA-V baseline. We compared the SMAP RDCA VOD with the SMOS VOD. We showed that even though there are differences in magnitude they have, in general, consistent temporal behavior tracking seasonal changes and strong spatial correlation.

Comparison of the SMAP RDCA VOD with tree height showed strong correlation and a linear relation especially for tree height less than 20 meters.

Comparison of the SMAP RDCA VOD with vegetation biomass showed moderate correlation. We also observed linear correlation for biomass less than 90 Mg/ha.

The magnitude of the SMAP RDCA VOD is comparable to the magnitude of the NDVI VOD due to the nature of the selection of the roughness parameter *h*. However, since the values of *h* are temporal invariant, the seasonality variation of the retrieved VOD should not be affected.

The application of temporal variant roughness parameter *h* should be explored for further improvement of the retrieved VOD.

ACKNOWLEDGMENT

This work is carried out by the Jet Propulsion Laboratory, California Institute of Technology, under a contract with the National Aeronautics and Space Administration.

The SMOS Data were obtained from the "Centre Aval de Traitement des Données SMOS" (CATDS), operated for the "Centre National d'Etudes Spatiales" (CNES, France) by IFREMER (Brest, France).

This research was supported in part by the U.S. Department of Agriculture, Agricultural Research Service. USDA is an equal opportunity provider and employer.

The research described in this publication also included measurements from the Long-Term Agroecosystem Research (LTAR) network. LTAR is supported by the United States Department of Agriculture.

The University of Salamanca team involvement in this study was supported by the Spanish Ministry of Science and Innovation (projects ESP2017- 89463-C3-3-R and PID2020-114623RB-C33), the Castilla y León Government (projects SA112P20 and CLU-2018-04) and the European Regional Development Fund (ERDF).

We would like to thank Heather McNairn of the Agriculture and Agri-Food Canada (AAFC) for her work managing the core validation sites Carman.

REFERENCES

[1] D. Entekhabi, E. Njoku, P. O'Neill, K. Kellogg, et al., "The Soil Moisture Active Passive (SMAP) Mission," *Proceedings of the IEEE*, Vol. 98, no. 5, May, 2010.

[2] P. O'Neill, E. Njoku, T. Jackson, S. Chan, R. Bindlish, J. Chaubell. SMAP algorithm theoretical basis document: level 2 & 3 soil moisture (passive) data products, Revision F, Jet Propulsion Lab., California Inst. Technol., Pasadena, CA, USA (2020). (JPL D-66480)

[3] Chaubell, M. J., Yueh, S. H., Dunbar, R. S., Colliander, A., Chen, F., Chan, S. K., Entekhabi, D., Bindlish, R., O'Neill, P. E., Asanuma, J., Berg, A. A., Bosch, D. D., Caldwell, T., Cosh, M. H., Holifield Collins, C., Martinez-Fernandez, J., Seyfried, M., Starks, P. J., Su, Z., … Walker, J. (2020). Improved SMAP Dual-Channel Algorithm for the Retrieval of Soil Moisture. IEEE Transactions on Geoscience and Remote Sensing, 58(6), 3894–3905. https://doi.org/10.1109/tgrs.2019.2959239

[4] A. Colliander, R.H. Reichle, W.T. Crow, M.H. Cosh, F. Chen, S. Chan, N. Das, R. Bindlish, J. Chaubell, S.B. Kim, Q. Liu, P. O'Neill, R.S. Dunbar, L. Dang, J. Kimball, T.J. Jackson, H.K. al Jassar, J. Asanuma, B. K. Bhattacharya, A. Berg, D.D. Bosch, L. Bourgeau-Chavez, T. Caldwell, J-C. Calvet, W. Dorigo, C. Holifield Collins, K.H. Jensen, S. Livingston, E. Lopez-Baeza, J. Martínez-Fernández, H. McNairn, M. Moghaddam, C. Montzka, C. Notarnicola, T. Pellarin, J. Prueger, J. Pulliainen, J. Ramos, M. Seyfried, P. Starks, Z. Su, Rogier van der Velde, Yijian Zeng, M. Thibeault, J.P. Walker, M. Zribi, D. Entekhabi, S. Yueh, "Validation of Soil Moisture Data Products from the NASA SMAP Mission", In preparation to submit to JSTAR, SMAP special issue, 2021.

[5] A. G. Konings, M. Piles, N. Das, D. Entekhabi, "L-band vegetation optical depth and effective scattering albedo estimation from SMAP". *Remote Sensing of Environment*, Vol. 198, pp. 460–470, 2017

[6] Y. H. Kerr et al., "The SMOS Mission: New Tool for Monitoring Key Elements of the Global Water Cycle," *Proceedings of the IEEE*, vol. 98, no. 5, pp. 666-687, May 2010.

[7] Heather Lawrence, J.-P. Wigneron, P. Richaume, N. Novello, J. Grant, A. Mialon, A. Al Bitar, O. Merlin, D. Guyon, D. Leroux, S. Bircher, Y. Kerr, "Comparison between SMOS Vegetation Optical Depth products and MODIS vegetation indices over crop zones of the USA", *Remote Sensing of Environment*, Vol. 140, pp. 396-406, 2014

[8] Rodríguez-Fernández, N. J., Mialon, A., Mermoz, S., Bouvet, A., Richaume, P., Al Bitar, A., Al-Yaari, A., Brandt, M., Kaminski, T., Le Toan, T., Kerr, Y. H., and Wigneron, J.-P.:,"An evaluation of SMOS L-band vegetation optical depth (L-VOD) data sets: high sensitivity of L-VOD to above-ground biomass in Africa", *Biogeosciences*, 15, 4627–4645, https://doi.org/10.5194/bg-15-4627-2018, 2018.

[9] J.P. Grant, J.-P. Wigneron, R.A.M. De Jeu, H. Lawrence, A. Mialon, P. Richaume, A. Al Bitar, M. Drusch, M.J.E. van Marle, Y. Kerr, "Comparison of SMOS and AMSR-E vegetation optical depth to four MODIS-based vegetation indices", *Remote Sensing of Environment*, Vol 172, pp. 87-100, 2016

[10] Fernandez-Moran, et al, SMOS-IC: An Alternative SMOS Soil Moisture and Vegetation Optical Depth Product. *Remote Sens.* Vol 9, pp. 457, 2017

[11]Mo, T., Choudhury, B., Schmugge, T., Wang, J., Jackson, T., 1982. A model for microwave emission from vegetation-covered fields. *Journal of Geophysical Research: Oceans*. Vol. 87(C13), pp. 11229–11237.

[12] O'Neill, P. E., S. Chan, E. G. Njoku, T. Jackson, R. Bindlish, and J. Chaubell. 2020. "SMAP Enhanced L2 Radiometer Half-Orbit 9 km EASE-Grid Soil Moisture, Version 4". Boulder, Colorado USA. NASA National Snow and Ice Data Center Distributed Active Archive Center. doi: https://doi.org/10.5067/Q8J8E3A89923.

[13] Simard, M., Pinto, N., Fisher, J., Baccini, A., "Mapping forest canopy height globally with spaceborne lidar", *Journal of Geophysical Research*, Vol. 116, G04021, Vol. 12 pp., 2011, doi:10.1029/2011JG001708

[14] Avitabile, V., Herold, M., Heuvelink, G. B. M., Lewis, S. L., Phillips, O. L., Asner, G. P., Armston, J., Ashton, P. S., Banin, L., Bayol, N., Berry, N. J., Boeckx, P., de Jong, B. H. J., DeVries, B., Girardin, C. A. J., Kearsley, E., Lindsell, J. A., Lopez-Gonzalez, G., Lucas, R., Malhi, Y., Morel, A., Mitchard, E. T. A., Nagy, L., Qie, L., Quinones, M. J., Ryan, C. M., Ferry, S. J. W., Sunderland, T., Laurin, G. V., Gatti, R. C., Valentini, R., Verbeeck, H., Wijaya, A. and Willcock, S. "An integrated pan-tropical biomass map using multiple reference datasets". Global Change Biology, Vol. 22. no. 4: pp. 1406–1420. Oct. 2016. doi:10.1111/gcb.13139

[15] A. Colliander, T.J. Jackson, R. Bindlish, S. Chan, N. Das, S.B. Kim, M.H. Cosh, R.S. Dunbar, L. Dang, L. Pashaian, J. Asanuma, K. Aida, A. Berg, T. Rowlandson, D. Bosch, T. Caldwell, K. Caylor, D. Goodrich, H. al Jassar, E. Lopez-Baeza, J. MartÃnez-FernÃ¡ndez, A. GonzÃ¡lez-Zamora, S. Livingston, H. McNairn, A. Pacheco, M. Moghaddam, C. Montzka, C. Notarnicola, G. Niedrist, T. Pellarin, J. Prueger, J. Pulliainen, K. Rautiainen, J. Ramos, M. Seyfried, P. Starks, Z. Su, Y. Zeng, R. van der Velde, M. Thibeault, W. Dorigo, M. Vreugdenhil, J.P. Walker, X. Wu, A. Monerris, P.E. O'Neill, D. Entekhabi, E.G. Njoku, S. Yueh, "Validation of SMAP surface soil moisture products with core validation sites", *Remote Sensing of Environment*, Vol. 191, pp. 215-231, March 2017.

[16] Schaefer, G. L., Cosh, M. H., & Jackson, T. J. "The USDA Natural Resources Conservation Service Soil Climate Analysis Network (SCAN)". *Journal of Atmospheric and Oceanic Technology*, Vol. 24, no. 12, 2007. https://doi.org/10.1175/2007JTECHA930.1

[17] Diamond, H. J., Karl, T. R., Palecki, M. A., Baker, C. B., Bell, J. E., Leeper, R. D., Easterling, D. R., Lawrimore, J. H., Meyers, T. P., Helfert, M. R., Goodge, G., & Thorne, P. W. "U. S. Climate Reference Network, after one decade of operations: Status and assessment". *Bulletin of the American Meteorological Society*, Vol. *94*, pp. 485–498, 2013 https://doi.org/10.1175/BAMS-D-12-00170.1

[18] Illston, B. G., Basara, J., Fischer, D. K., Elliott, R. L., Fiebrich, C., Crawford, K. C., Humes, K. S., & Hunt, E. "Mesoscale monitoring of soil mositure across a statewide network." *Journal of Atmospheric and Oceanic Technology*, Vol. *25*, pp. 167–182, 2008

[19] Smith, A. B., J. P. Walker, A. W. Western, R. I. Young, K. M. Ellett, R. C. Pipunic, R. B. Grayson, L. Siriwardena, F. H. S.Chiew, and H. Richter (2012), "The Murrumbidgee soil moisture monitoring network data set", *Water Resour. Res.*, 48, W07701, doi:10.1029/2012WR011976.

[20] Tetlock E, Toth B, Berg A, Rowlandson T, Ambadan JT. (2019). "An 11-year (2007–2017) Soil Moisture and Precipitation Dataset from the Kenaston Network in the Brightwater Creek Basin, Saskatchewan, Canada". *Earth System Science Data*, Vol. 11, No. 2, pp. 787-96. https://doi.org/10.5194/essd-11-787-2019

[21] Bhuiyan, H.A., McNairn, H., Powers, J., Friesen, M., Pacheco, A., Jackson, T.J., Cosh, M.H., Colliander, A., Berg, A., Rowlandson, T., Bullock, P. and Magagi, R. (2018), "Assessing SMAP Soil Moisture Scaling and Retrieval in the Carman (Canada) Study Site". *Vadose Zone Journal*, 17: 1-14 180132. doi:10.2136/vzj2018.07.0132

[22] Bircher, S., N. Skou, K. H. Jensen, J. P. Walker, and L. Rasmussen. "A soil moisture and temperature network for SMOS validation in Western Denmark", *Hydrol. Earth Syst.* Sci., Vol. 16, pp. 1445–1463, https://doi.org/10.5194/hess-16-1445-2012, 2012.

[1]Martinez-Fernandez, J., A. Ceballos, "Mean Soil Moisture Estimation Using Temporal Stability Analysis," Vol. 312, pp. 28-38, 2005. doi:10.1016/j.jhydrol.2005.02.007

[2]van der Velde, R., Colliander, A., Pezij, M., Benninga, H.-J. F.,Bindlish, R., Chan, S. K., Jackson, T. J., Hendriks, D. M. D., Augustijn, D. C. M., and Su, Z. (2021). Validation of SMAP L2 passive-only soil moisture products using upscaled in situ measurements collected in Twente, the Netherlands, Hydrol. Earth Syst. Sci., Vol. 25, pp. 473–495, doi: 10.5194/hess-25-473-2021, 2021.

[25] Keefer, T. O., M. S. Moran, and G. B. Paige, 2008: "Long-term meteorological and soil hydrology database, Walnut Gulch experimental. watershed, Arizona, United States". *Water Resour. Res*., 44, W05S07, https://doi.org/10.1029/2006WR005702.

[26] Bosch, D. D., J. M. Sheridan, R. R. Lowrance, R. K. Hubbard, T. C. Strickland, G. W. Feyereisen, and D. G. Sullivan, 2007: "Little River experimental watershed database". *Water Resour. Res*., 43, W09472, https://doi.org/10.1029/2006WR005844.

[27] Seyfried, M. S., Lohse, K. A., Marks, D., Flerchinger, G. N., Pierson, F., Holbrook, S. (2018): "Reynolds Creek Experimental Watershed and Critical Zone Observatory". *Vadoze Zone Journal* 17:180129. DOI: 10.2136/vzj2018.07.0129

[28] Coopersmith, E., Cosh, M. H., Petersen, W. A., Prueger, J. H., & Niemeier, J. J. (2015). "Soil moisture model calibration and validation: An ARS watershed on the South Fork Iowa River". *Journal of Hydrometeorology*, Vol. 16, 1087–1101.

[29] Starks, P. J., J. L. Steiner, and A. J. Stern, 2014: "Upper Washita River experimental watersheds: Land cover data sets (1974–2007) for two southwestern Oklahoma agricultural watersheds". *J. Environ. Qual*., 43, 1310–1318, https://doi.org/10.2134/jeq2013.07.0292.

[30] Caldwell, T. G., T. Bongiovanni, M.H. Cosh, T.J. Jackson, A. Colliander, C.J. Abolt, R. Casteel, T. Larson, B.R. Scanlon, M.H. Young. (2019). "The Texas Soil Observation Network: A comprehensive soil moisture dataset for remote sensing and land surface model validation". *Vadose Zone J*. Accepted Paper. https://doi.org/10.2136/vzj2019.04.0034